Dynamics and energetics of the $K(^2S) + H_2(X^1\Sigma_g^+)$ reaction: Significance of orientational and (ro)vibrational contribution

Santhakumar Yeswanth Kumar [a], Natarajan Arumugam [b], Abdulrahman I. Almansour [b], Muhammed Jeneesh Kariyottu Kuniyil [c], Ramanathan Padmanaban [a,*]

[a] Department of Chemistry, School of Physical Chemical and Applied Sciences, Pondicherry University, Puducherry 605 014, India
[b] Department of Chemistry, College of Science, King Saud University, P.O. Box 2455, Riyadh 11451, Saudi Arabia
[c] Institute of Nanotechnology, Karlsruhe Institute of Technology (KIT), Hermann-von-Helmholtz-Platz 1, 76344 Eggenstein-Leopoldshafen, Karlsruhe, Germany

Keywords:
Coriolis coupling
Centrifugal sudden
Time-dependent wavepacket

A B S T R A C T

The significance of orientational and (ro)vibrational excitations on the $K(^2S) + H_2(X^1\Sigma_g^+)$ reaction dynamics is presented here by performing the exact time-dependent wavepacket calculations using the Coriolis coupling (CC) approach. Employing the new accurate *ab initio* ground electronic surface $1\ ^2A'$ reported by Yuan *et al.* (2018), the dynamical quantities such as integral cross sections and thermal rate constants are computed within the CC and CS (centrifugal sudden) methods. All partial wave contributions of J (total angular momentum) up to 90 are required to get the convergence in dynamical results up to the collision energy of 3.5 eV. The present study attests that the ground and first vibrational level dynamics is insignificant. For $v = 2$, the reaction probability is monotonically increasing, followed by the onset noted near 1.25 eV, as a function of collision energy up to 3.5 eV. Further, the kinematic effects (replacing H by D atom) on the title system is also performed and found that the KH product formation is more favored than the KD product via HD depletion path.

1. Introduction

Space is filled with numerous gas elements and the detection of interstellar neutral potassium (40K) was first reported by Dunham and coworkers in 1937 towards 188 early-type stars [1]. Ever since the introduction of reaction dynamics in chemistry, numerous research have been undergone for AH_2 (A = alkali atom) systems which are significant in the interstellar collision dynamics. Reactions of alkali elements with molecular hydrogen had great attention and studied extensively in both theoretical and experimental way. Especially, the study of lithium with molecular hydrogen and its reverse reaction have evolved much attention in studying the formation and depletion processes of LiH molecules which plays significant role in the formation of universe [2–4]. There are also some experimental reports on A + H_2 (A = Na to Cs) systems [5–8] which indicate that these reactions are highly endothermic in the ground electronic state and the endothermicity values increase with the increasing atomic mass of the element A. Further, the atomic size of group I elements plays significant role in establishing its preference of approach in the reactive pathway [8]. As the group I elements comprises of both lighter (Li and Na) and heavier alkali atoms (K, Rb, and Cs), the reaction mechanisms of A + H_2 are expected to be different for different alkali elements. In case of lighter atoms, the preferential attack to H_2 goes along a side-wise which effectively follows the surface hopping model, whereas the heavier atoms prefer to approach H_2 through collinear geometry via an electron transfer which follows a harpoon model [8].

The title reaction, $K(^2S) + H_2(X^1\Sigma_g^+)$ is of endothermic type with endoergicity about 2.62 eV, which is relatively high to facilitate the collision. Therefore, the intake of energy has to be drawn either from a large collisional or vibrational contribution which makes it very tedious to carry out the experimental study. The history of investigating KH_2 system dates back to 1980s, where Lin *et al.* [9] experimentally carried out the collisional deactivation of electronically excited alkali atom ("superalkali") $K(5^2P_J)$ by H_2 molecule using the time-resolved fluorescence and atomic absorption techniques. It yields KH + H with the potassium in one of its lower electronic states such as $5^2S_{1/2}$, $4^2S_{1/2}$ via quenching process. To produce the $K(5^2P_J)$ source, they have used the pulsed photo-dissociation of KI at 193 nm, and it is discovered that this reaction has little bearing on the deactivation process of KI. Some more experimental studies of collision between an electronically excited alkali atom with H_2 molecules, involving pump-probe method in low-pressure heat pipe oven experiment, report that they were of

* Corresponding author.
E-mail address: rpn.che@pondiuni.edu.in (R. Padmanaban).

greater exothermicity towards the selective production of KH [10–14] For the K+H_2 reaction, the influence of various rovibrational (v, j) state and its distribution turning into translational, vibrational and rotational levels of product KH were determined. They have reported that the reaction via collinear abstraction process follows harpoon mechanism involving the formation of ion-pair intermediate complex (K^+HH^-) which is found to be more dominant [7,10,11,15–19]. In 1999, Wong *et al.* [20] have reported the chemical dynamics of KH_2 reaction by obtaining the scattering state spectrum which was found to be the superior reaction passing over a small activation barrier by electron jump mechanism. Later in 2000, Hsiao *et al.* , calculated the activation energy of reaction occurring between excited potassium atom [15] K($6s^2$S), K($7s^2$S) and K($8s^2$S) with hydrogen molecule. The obtained results showed similar heights of the potential barrier predicted by linear geometry approach.

According to the above discussions, the history of studying K + H_2 collisions is extensive in experiments and there is no further experimental results reported recently on the reaction involving ground state K atom, i.e., $K(^2S) + H_2(X^1\Sigma_g^+) \rightarrow H_2 + KH(X^1\Sigma^+)$. In case of the dynamical study of such collision in theoretical point of view, potential energy surface (PES) plays a major role where the construction of global PES is a tedious task. So far, unavailability of suitable ground state PES which led to the inefficiency in advancement of dynamical and resonance results in the literature. Very recently, Li *et al.* had reported the first new diabatic PESs for the ground and first excited electronic states for the $K(4p^2P) + H_2(v_0 = 0, 1,\ j_0 = 0)$ [21]. They have claimed that the vibrational excitation played a significant role in promoting the reaction than the translational energy of H_2 reagent, and further the direct abstraction mechanism was dominant at the state-to-state level. The availability of another two newly constructed PESs, one adiabatic by Yuan *et al.* [22] and another one is non-adiabatic by Li *et al.* ended up to carry out the present study. They have also studied the dynamics using quasi-classical trajectory (QCT) method for the K + $H_2(v = 0 - 2, j = 0)$ reagents, and discovered that the collision process may be efficiently accelerated by the vibrationally "hot" H_2 molecules. In 2020, Li *et al.* done nonadiabatic dynamics of $K(4p^2P)$ + $H_2(X^1\Sigma_g^+)$ reaction on their newly reported PES, considering first electronic excited state ($2^2A'$) in the state-to-state level of theory. The dynamical findings shows that the vibrational excitation of H_2 was substantially more effective than the translational energy at facilitating the reaction. Furthermore, the differential cross-sections showed forward-biased scattering, suggesting that the direct abstraction mechanism in the reaction dominates the reaction. Hence, the present work evident the dynamical study of K(^{2}S) + H_2 reaction employing a new PES constructed by Yuan *et al.* [22] (hereafter YDWLH PES) using time-dependent wavepacket approach (TDWP). The employed YDWLH PES was constructed by internally contracted multi-reference configuration interaction (MRCI) with complete active space self-consistent field (CASSCF) uses AV5Z basis set for H atom and QZVPP was used for K atom. Neural network method was applied to fit the constructed PES, and the obtained bond parameters was well in agreement with available experimental data.

In this work, the extensive dynamical calculations are performed for the K + H_2 reaction employing YDWLH PES [22] and reported the initial state-selected observable such as cross sections and rate constants. The results obtained within the centrifugal sudden (CS) approximation are validated with the exact approach which includes the Coriolis coupling (CC) elements. Further, the kinematic effects on the reaction dynamics is also performed and compared the results for the vibrationally hot HD and D_2 reagents. The paper is organized as, the theoretical methods (Section 2) followed by the results and discussions (Section 3), and then summarize the present work.

2. Theoretical methods

In this section, to extract the reactive scattering dynamical attributes such as reaction probabilities, integral cross section, thermal rate constants of K + H_2 collision, we have presented a well established TDWP method [23–27]. Here, the first step is to solve the time-dependent Schrödinger equation (TDSE) numerically using the mass-scaled Jacobi coordinates (R, r, γ) in the body-fixed (BF) frame along z-axis. R and r are the Jacobi distances and γ represents the approaching angle of incoming K atom to the center of mass of H_2 molecule. Initially, the wavefunction at time $|\Psi(t)\rangle$ which has the time-independent Hamiltonian operator $(\hat{H})$ is given by:

$$|\Psi(t)\rangle = \exp\left[-i\hat{H}t/\hbar\right]|\Psi(t=0)\rangle, \tag{1}$$

$$\hat{H} = -\frac{\hbar^2}{2\mu}\left[\frac{\partial^2}{\partial R^2} + \frac{\partial^2}{\partial r^2}\right] + \frac{\hat{j}^2}{2\mu r^2} + \frac{\hat{l}^2}{2\mu R^2} + V(R, r, \gamma), \tag{2}$$

where, the quantity μ is the three-body scaled reduced mass of the K + H_2 system.

In relation to R, the orbital angular momentum operator $(\hat{l})$ is expressed in terms of the total angular momentum operator $(\hat{J})$ and the diatomic rotational angular momentum operator $(\hat{j})$ as,

$$\hat{l}^2 \equiv (\hat{J} - \hat{j})^2 = \hat{J}^2 + \hat{j}^2 - 2\hat{J}_z\hat{j}_z - \hat{J}_+\hat{j}_- - \hat{J}_-\hat{j}_+ \tag{3}$$

where $\hat{J}_z$ and $\hat{j}_z$ are corresponding BF z component and $\hat{J}$ is the operator for total angular momentum. The diatom $\vec{r}$ is preserved in the (x, z) plane while the BF z-axis is defined along the Jacobi vector $\vec{R}$, the analogous to raising (lowering) operators $\hat{J}_+(\hat{J}_-)$ and $\hat{j}_+(\hat{j}_-)$. These last two terms in Eq. (3) are known as Coriolis coupling terms [28–31]. Neglecting the CC terms result into the CS approximation [32,33], and in the present study we performed the calculations explicitly, for the both methods, for all partial waves J up to its maximum quantum number J_{max}.

Upon consideration of projection of J (including j) quantum number (Ω onto the BF z-axis), the coupling is established with Ω and $\Omega\pm1$ substates. Effect of CC is evaluated for each Ω, where the Ω is restricted to non-negative values which varies from 0 to Ω_{max} or $\min(J, j)$ with inclusion of degeneracy factor $(g\Omega)$. In short, the CC terms $(C^{\pm}_{J,j,\Omega})$ are expressed in form of tri-diagonal matrix as,

$$\begin{bmatrix} C_{J,j,0} & C^+_{J,j,0} & 0 & \dots & 0 \\ C^-_{J,j,1} & C_{J,j,1} & C^+_{J,j,1} & \ddots & \vdots \\ 0 & \ddots & \ddots & \ddots & 0 \\ \vdots & \ddots & C^-_{J,j,\Omega_{\max}-1} & C_{J,j,\Omega_{\max}-1} & C^+_{J,j,\Omega_{\max}-1} \\ 0 & \dots & 0 & C^-_{J,j,\Omega_{\max}} & C_{J,j,\Omega_{\max}} \end{bmatrix} \Longrightarrow \begin{pmatrix} \Psi^{J,\Omega=0} \\ \Psi^{J,\Omega=1} \\ \vdots \\ \Psi^{J,\Omega_{\max}-1} \\ \Psi^{J,\Omega_{\max}} \end{pmatrix} \tag{4}$$

For clarity, the prefactor $\hbar^2/2\mu R^2$ is not included in the above matrix, and the corresponding diagonal and off-diagonal $(\pm)$ elements (eigenvalues) are given as:

$$C_{J,j,\Omega} = J(J+1) + j(j+1) - 2\Omega^2 \tag{5}$$

$$C^{\pm}_{J,j,\Omega} = -[J(J+1) - \Omega(\Omega\pm1)]^{1/2}\,[j(j+1) - \Omega(\Omega\pm1)]^{1/2}. \tag{6}$$

This affects the centrifugal or the effective potentials caused by the action of $\hat{l}^2$ operator's interaction with the wavefunction $\Psi^{J\Omega}$ in the (R, r, γ) grid space at a given time t.

For the motion along the corresponding R, r, Ω and the product translation, vibrational (v, j) and we use normalized associated Legendre polynomials (angular) functions and are given as

$$|\Psi^{J\Omega}(R, r, \gamma, t=0)\rangle = \sqrt{w_n}\ F(R)\ \phi_{vj}(r)\ \tilde{P}^{\Omega}_j(\cos\gamma). \tag{7}$$

In the above wavefunction, the translational part $F(R)$, is considered from the minimum uncertainty Gaussian WP (GWP) as

$$F(R) = \left(\frac{1}{2\pi\delta^2}\right)^{\frac{1}{4}} \exp\left[-\frac{(R-R_0)^2}{4\delta^2} - ik_0(R-R_0)\right], \tag{8}$$

where, δ is the width parameter of the GWP and $R_0(k_0)$ is the location of its maximum in the coordinate(momentum) space. The detailed

explanation of how the theoretical scheme is done can be found in our previously published paper [34].

Once the construction of WP is done, then the propagation of WP has to take place, here we use second order split-operator method to propagate the WP,

$$e^{-i\hat{H}\Delta t/\hbar} = e^{-iV\Delta t/2\hbar}\ e^{-i\hat{T}_\gamma \Delta t/2\hbar}\ e^{-i\hat{T}_r \Delta t/\hbar}\ e^{-i\hat{T}_\gamma \Delta t/2\hbar}\ e^{-iV\Delta t/2\hbar} + O[(\Delta t^3)], \quad (9)$$

where, $\hat{T}_r$ is the total radial operator (in the R and r coordinates) and $\hat{T}_\gamma$ is the total angular operator (in the γ coordinate) in kinetic energy operators respectively. The exponential containing wavefunction is further evaluated by fast Fourier transformation (FFT) [23] and discrete variable representation (DVR). To avoid reflections of the WPs in the asymptotic regions of the both reactant and product channel, sine-type damping functions [35] were used at the boundaries, and finally we obtain the flux.

From the obtained flux, the energy-resolved reaction probability is extracted in form of $P_{vj}^{J\Omega}(E)$

$$P_{vj}^{J\Omega}(E) = \langle \Phi(R,r,\gamma,E)|\hat{F}|\Phi(R,r,\gamma,E)\rangle|_{r=r_d}, \quad (10)$$

$$= \frac{\hbar}{\mu}\mathrm{Im}\left[\left\langle \Phi(R,r_d,\gamma,E)\middle|\frac{\partial\Phi(R,r_d,\gamma,E)}{\partial r}\right\rangle\right]\Big|_{r=r_d}. \quad (11)$$

For a given collision energy at a specific (v,j) level of the H_2 reagent, upon adding the reaction probabilities, the initial state-selected energy-resolved reaction cross-section is determined (cf. Eq. (11)) across J and Ω quantum numbers.

$$\sigma_{vj}(E) = \frac{\pi}{k'^{\,2}_{vj}}\left(\sum_{\Omega=0}^{\Omega_{max}} \frac{g_\Omega}{(2j+1)} \sum_{J\geq\Omega}^{J_{max}} (2J+1) P_{vj}^{J\Omega}(E)\right), \quad (12)$$

where, g_Ω is the degeneracy factor which carries the value 1 (for $\Omega = 0$) or 2 (for $\Omega \neq 0$). k'_{vj} quantity in Eq. (12) refers to the translational energy component obtained from the initial rovibrational energy of H_2 molecule (ϵ_{vj}) as, $[\sqrt{2\mu(E-\epsilon_{vj})}/\hbar]$. The rovibrational energies can be found in the supporting information, Table S1.

The initial state-selected temperature dependent rate constant, $k_{vj}(T)$ is obtained on averaging the energy-resolved cross section [cf. Eq. (12)] over the Boltzmann distribution of energy,

$$k_{vj}(T) = \left(\frac{8k_BT}{\pi\mu}\right)^{1/2} \frac{1}{(k_BT)^2} \int_0^\infty E_{tr}\ \sigma_{vj}(E_{tr})\ e^{-E_{tr}/k_BT}\, dE_{tr}, \quad (13)$$

where k_B is the Boltzmann constant. When we average the k_B over the Boltzmann distribution of population in the rotational levels, we get the j-state averaged accurate rate constant:

$$k_v(T) = \sum_j g_{el}\ \frac{(2j+1)}{Q_{int}(T)} e^{-\epsilon_{vj}/k_BT}\ k_{vj}(T), \quad (14)$$

where, $Q_{int}(T)$ is the internal reagent partition function includes vibrational and rotational part of H_2 molecule. All the information with regard to WP and the numerical grid used in the calculations are given in Table 1.

Table 1
Numerical grid parameters and properties of the initial WP used in the TDWP calculations. The units used here are given within the parenthesis.

Parameter	Value	Description
$N_R/N_r/N_\gamma$	512/128/48	Number of grid points
R_{min}/R_{max} (a_0)	1.0/39.325	Extension of the grid along R
R_{mask}/r_{mask} (a_0)	33.70/4.90	Starting point of the masking function
r_{min}/r_{max} (a_0)	0.1/6.45	Extension of the grid along r
$\Delta R/\Delta r$ (a_0)	0.075/0.05	Grid spacings along R and r
r_d (a_0)	4.10	Location of the dividing surface in the product channel
E_{trans} (eV)	2.0	Initial translational kinetic energy
R_0 (a_0)	27.0	Initial location of the center of the GWP
δ (a_0)	0.15	Initial width parameter of the GWP
Δt (fs)	0.6465	Time step used in the WP propagation
T (fs)	2647	Total propagation time
$\langle\Psi(t)\|\Psi(t)\rangle$	0.000108	Norm of the WP at the final time (for $J=0$)

3. Results and discussion

3.1. Minimum energy profile and the effective potential

In this section, we present the results obtained from the quantum dynamical calculations for the $K(^2S) + H_2(X^1\Sigma_g^+)$ reaction using the YDWLH PES [22] and they are discussed in detail. The accurate ground electronic PES ($^2A'$) of KH_2 system [22] features the spectroscopic constants such as equilibrium distance, dissociation energy, and zero point energy (ZPE), which describes the experimental data [36,37] precisely for $H_2(X^1\Sigma_g^+)$ and with some discrepancies for $KH(X^1\Sigma^+)$ molecule. Here, a noticeable difference between the dissociation energy of reactant H_2 (4.734 eV) and product KH molecule (1.79 eV) leads the title reaction to be highly endothermic, and the endoergicity is about 2.95 eV with reference to the energy minimum. A schematic diagram of minimum energy profile of underlying PES representing the both reactant and product asymptotes is shown in Fig. 1, for different approaching angle (γ = 30–180). As stated above, a significant amount of energy is required to initiate the $K + H_2$ reaction due to its endothermic nature, where the reactivity was highly influenced by the vibrational excitations rather than the translational energy. It means that the vibrationally excited H_2 molecule extends its bond length and makes the abstraction of H easier by the incoming K atom to yield the product KH molecule. It can be seen from Fig. 1 that the reaction proceeds without any barrier and it therefore becomes straightforward. The zero energy scale in the figure represents the minimum potential of H_2 at the asymptotic reactant channel (i.e., $R \to \infty$).

Since the present study includes the CC terms [cf. (6)] in the dynamics, it is worth to first see the role of these terms on the effective potential which adds a centrifugal barrier to the title system. In Fig. 2, we have plotted the $1D$-cut of effective potential, V_{eff}, as a function of R coordinate for different J (panel (a)), j (panel (b)), and Ω (panel (c)) states for the vibrationally excited reagent $H_2(v=2)$. In this figure, the solid line represents the V_{eff} including the CC terms, whereas the dashed line represents the V_{eff} arises only due to the diagonal terms (CS approximation). From Fig. 2(a), increasing J perturbs the energy minimum and gradually shifts it to higher energy, and finally the surface attains a repulsive nature when J reaches its maximum (J_{max} = 90). The double well feature seen in Fig. 2(c) at low J and j values is gradually disappearing upon increasing J. Unlike the J and j quantum numbers, the projection quantum number Ω do not contribute significantly to the V_{eff}. Among three different rotation, the diatomic rotation j contribution is major in V_{eff}, and the three-body rotational quantum number J shifts the whole collision to longer R (direct scattering).

3.2. Reaction probabilities

The initial state-selected and energy-resolved (integrated all open product (v',j') states at a given energy) reaction probabilities for the $K + H_2(v = 0\text{–}3, j = 0)$ reaction is shown in Fig. 3 for $J = 0$ at the collision energy range of 1.0–3.5 eV. It is clearly witnessed from figure that the reaction is not facilitated by the ground vibrational level of reagent H_2 (see the inset of Fig. 3), and the reaction probability shows some marginal increase (~5%) even at high energy for the first $v = 1$ level. The plausible reason for this is that the energy required to reach the product (KH) channel from zero vibrational level of H_2 reactant channel is significantly high, ~2.95 eV, as featured by the employed YDWLH-PES. So, the reaction triggers only from the $v = 2$ level with sufficient vibrational energy to reach the interaction region where the formation of the KH_2 complex happens. Therefore, $v = 2$ is considered here as the minimum vibrational quanta to initiate the $K + H_2$ collision, and noted the significance of vibrational excitations. Since the reagent diatom is homonuclear type, only the KH product is

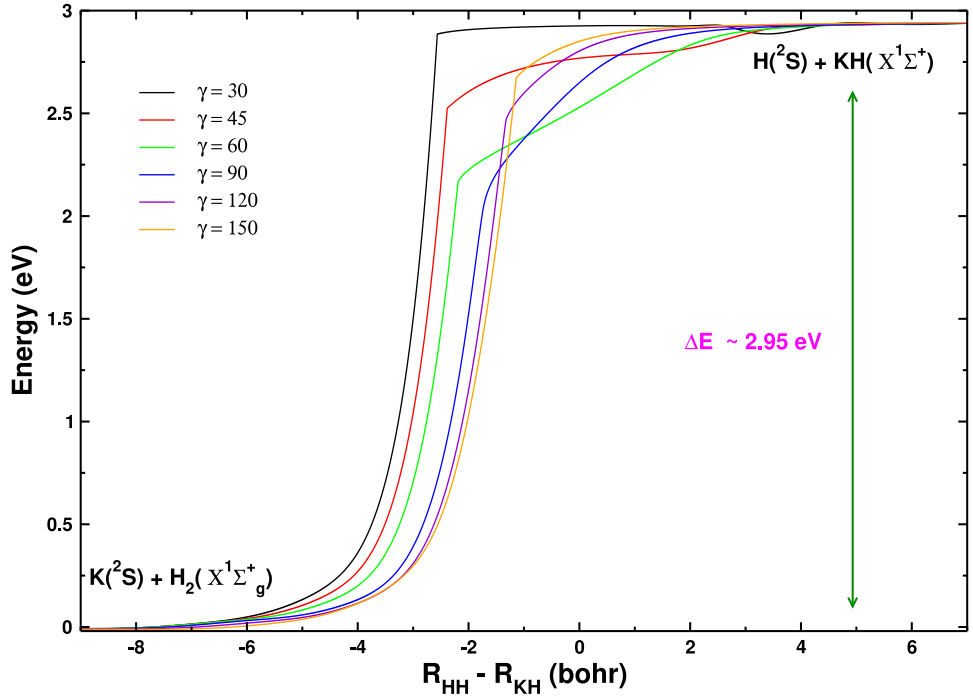

Fig. 1. Minimum energy profile of the K + H_2 reaction for different Jacobi angles (γ), shows the endoergicity of ~2.95 eV.

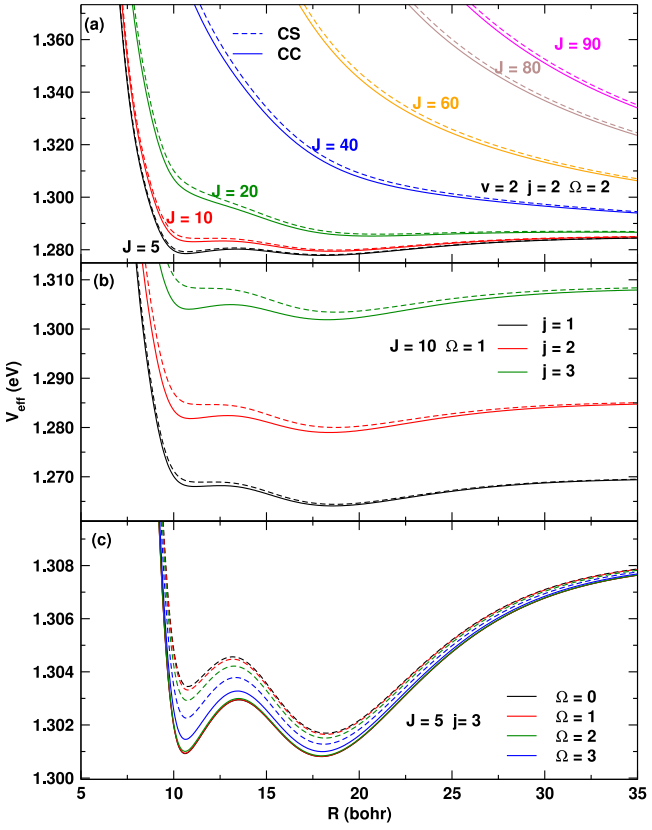

Fig. 2. 1D-cut of effective potential for different orientational ($J\Omega$) and rotational (j) contributions of the KH_2 system.

expected via the possible pathways: insertion type or collinear type. The reaction probability for ($v = 2, j = 0$) (green curve in Fig. 3) is slightly raised near the onset (E_{col} = 1.0–1.75 eV) and then monotonically increases with increasing collision energy. It exhibits some significant oscillations up to E_{col} ~ 3.0 eV which are latter identified as dynamical resonances of KH_2 complex. Going further high v level of H_2 reagent, the reaction probability increases linearly with v (probability is nearly 40% for $v = 3$), and the reactant enters the interaction region earlier to form the KH_2 complex. The effect of reagent rotations is also studied for the K + H_2(v = 2, j = 0–3) reaction, as shown in Fig. 4. It is verified again that the j-excitation is still insufficient to facilitate reaction when the H_2 reagent is in its ground vibrational level ($v = 0$). On the other hand, the rotational excitations significantly increase the reactivity when $v = 2$, and show the similar trend as seen in the reaction probability for ($v = 2, j = 0$). It is further noticed that $j = 3$ suppresses the oscillatory features and favors the direct scattering.

The J-dependent reaction probabilities, $P_{vj}^{J\Omega}(E)$, for K + H_2(v = 2, $j = 0$) reaction are extracted for a fixed projection quantum number $\Omega = 0$ within the CS approximation, and they are presented in Fig. 5. All partial waves of J up to 90 are considered in order to seek the convergence in the dynamical results for the collision energy up to ~3.5 eV. The convergence of all the calculations to extract reaction probability is done by the carefully chosen numerical grid parameters (see Table 1). As J increases, the reaction probability gradually decreases as a function of collision energy and it is almost suppressed to zero for $J_{max} = 90$. Further, the initial threshold (onset of the reaction) and the resonance features observed at lower J values are disappeared or rather shifted to higher energy. This is due to the centrifugal barrier added to the system potential [cf. Fig. 2] which influences the reaction to follow a more direct path, bypassing the formation of KH_2 intermediate complex.

Now, the projection quantum number Ω (varies from 0 to $\Omega_{max} = 2$) is taken into consideration in order to illustrate the role of CC in the reaction dynamics of the K + H_2 system which is achieved by permitting the coupling within the nearby substates, i.e., $\Omega\pm1$. Let us directly discuss the $j = 2$ results, which encounters the maximum Ω-coupling for the K + H_2 reaction. Note that for Ω_{max} = 2, the coupling is defined as $\Omega_0 \leftrightarrow \Omega_1$ (for Ω = 0), $\Omega_0 \leftrightarrow \Omega_1 \leftrightarrow \Omega_2$ (for Ω = 1), and $\Omega_2 \leftrightarrow \Omega_1$ (for Ω = 2). The initial state-selected $J\Omega$-dependent reaction probabilities for the K + H_2(v = 2, j = 2) system, extracted

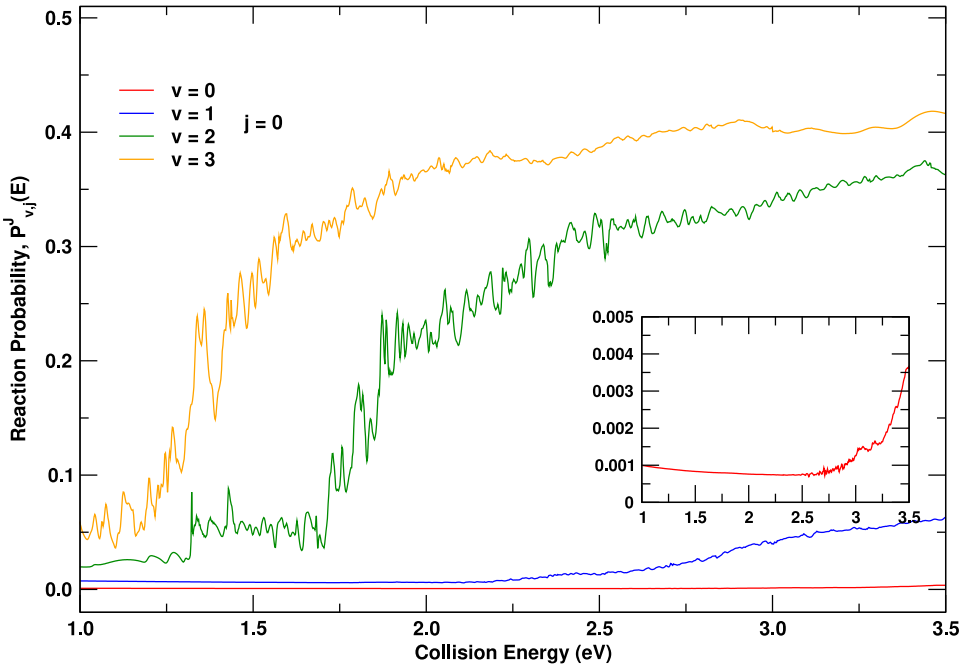

Fig. 3. Initial state-selected and energy-resolved reaction probabilities for K + H_2(v = 0–3, j = 0) system, plotted as a function of collision energy up to 3.5 eV. The enlarged probability curve for $v = 0$ is kept in the inset for clarity.

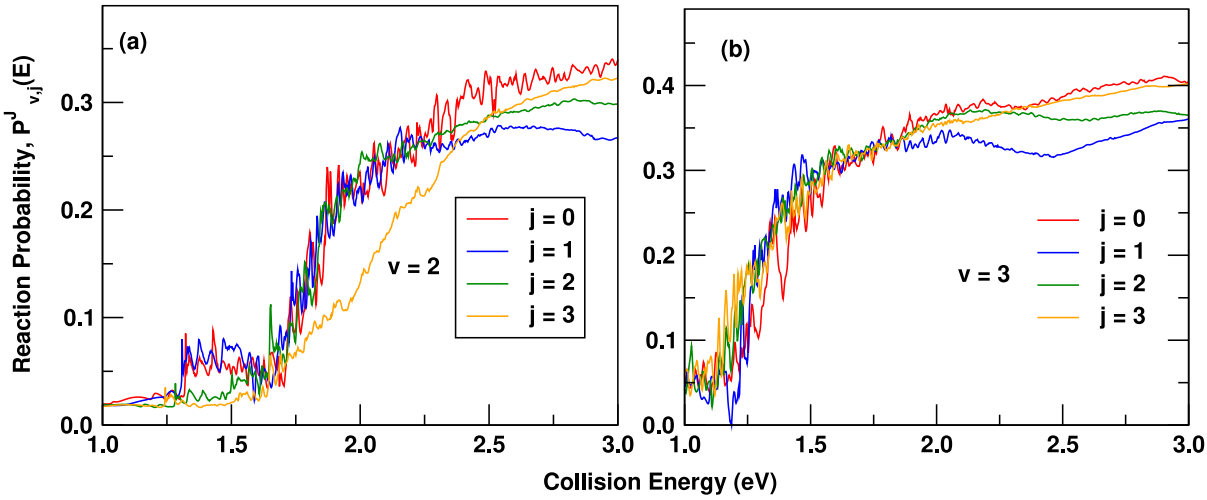

Fig. 4. The initial state-selected reaction probabilities for different rotational excitations for $v = 2$ (a) and $v = 3$ (b) of the H_2 reagent.

from CC and CS calculations, are presented in Fig. 6 for the selected J values (10, 30, 50, 70, and 90) and for $\Omega = 0$ ((a)–(e)), $\Omega = 1$ ((f)–(j)), and $\Omega = 2$ ((k)–(o)). The green and red solid lines represent the CC and CS results, respectively. The Ω-dependent reaction probability shows a similar trend as observed for $J \neq 0$ (see Fig. 5). The dense oscillations observed in the low energy range are greatly vanished at higher energies (above 3.0 eV), in both methods, which proves that it undergoes direct mechanism in absence of intermediate complex.

The Fig. 6 reveals that the Ω coupling is strongly influence the reactivity for high-J values compared to the low-J values, on the other hand the CC reaction probabilities for $\Omega = 2$ dominates the reactivity for all J values, compared to that of the CS result. Incidentally, the CS method reproduces the CC reaction probability for $J = 10$ and competes with the CC in favoring of reactivity for the specified initial state (v = 2, j). It continues for J up to 20 and then reduces the probability from collision energy above 1.5 eV. At high-J values (above 30), CS significantly reduces the probability values compared to the exact CC result. As one increase the Ω value, the system entitled for more coupling of rotational substates, i.e., $\Omega - 1 \leftrightarrow \Omega \leftrightarrow \Omega + 1$, within the range of 0 to $min(J, j)$. Therefore, the reactivity for the KH product formation is significantly favored when considering more Ω terms in the dynamics compared to that of the CS method in which those coupling ($\Omega \pm 1$) are neglected. Reaction probability values diminished to zero when the title system chooses its maximum orientations (J_{max} and Ω_{max}), and further the oscillations present in CS probability vanished much before the CC does. In conclusion, the K + H_2 system requires a sufficiently high vibrational and translational contribution and also includes more rotational states (high J and Ω) towards the selective formation of KH

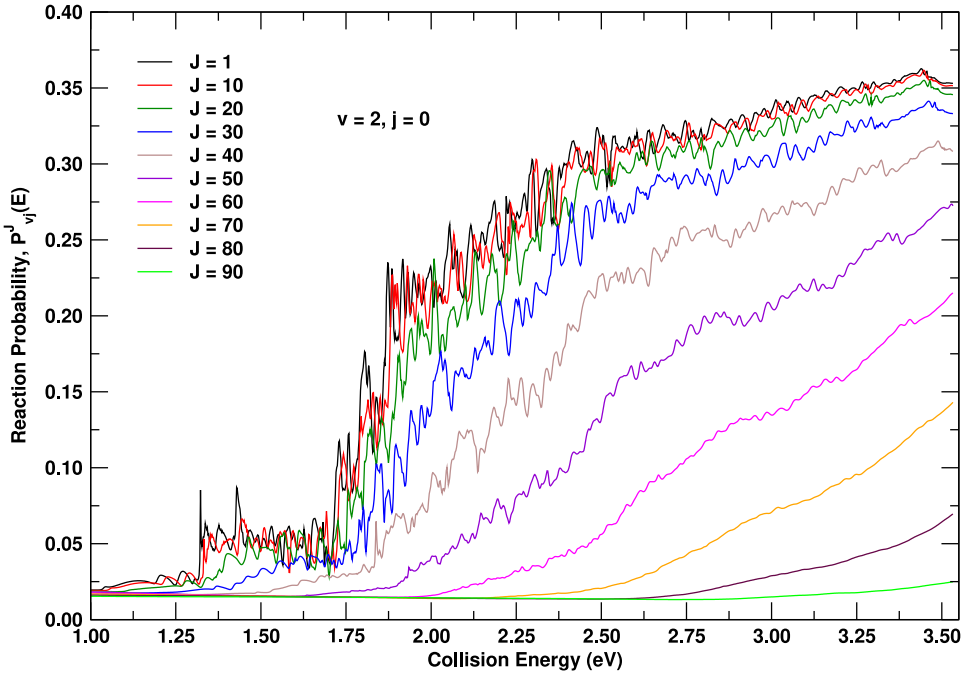

Fig. 5. J-dependent reaction probabilities as a function of collision energy for the K + $H_2(v = 2, j = 0)$ reaction.

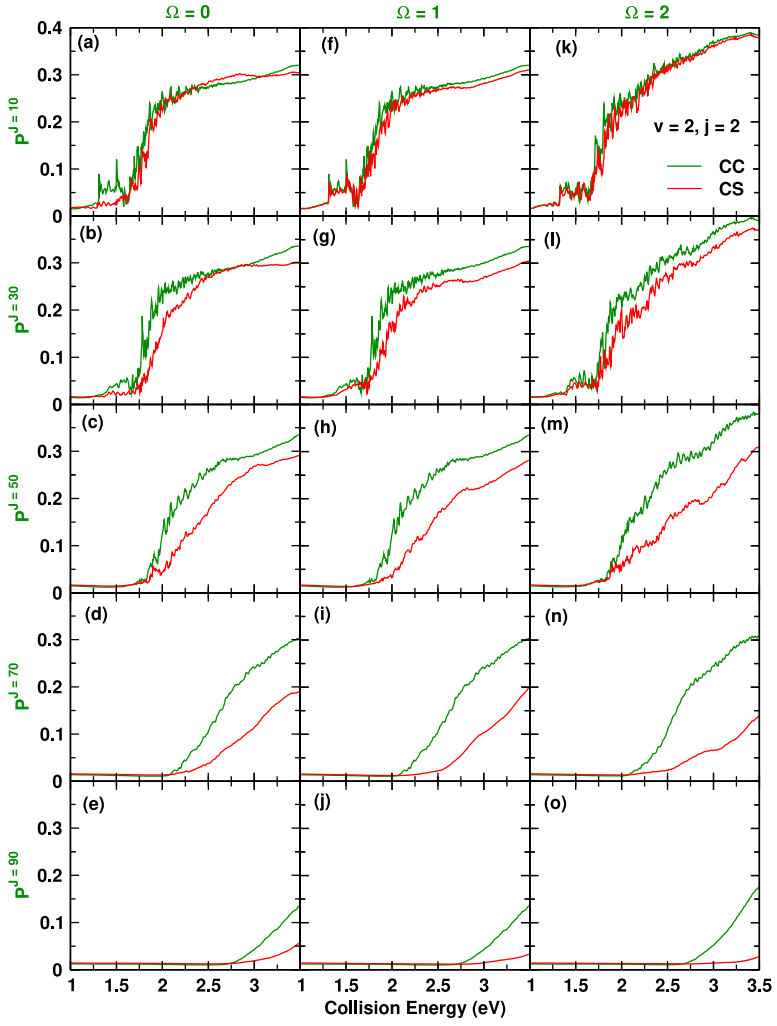

Fig. 6. The CC and CS probabilities for different J and Ω states (as indicated in figure) are compared for K + $H_2(v = 2, j = 2)$.

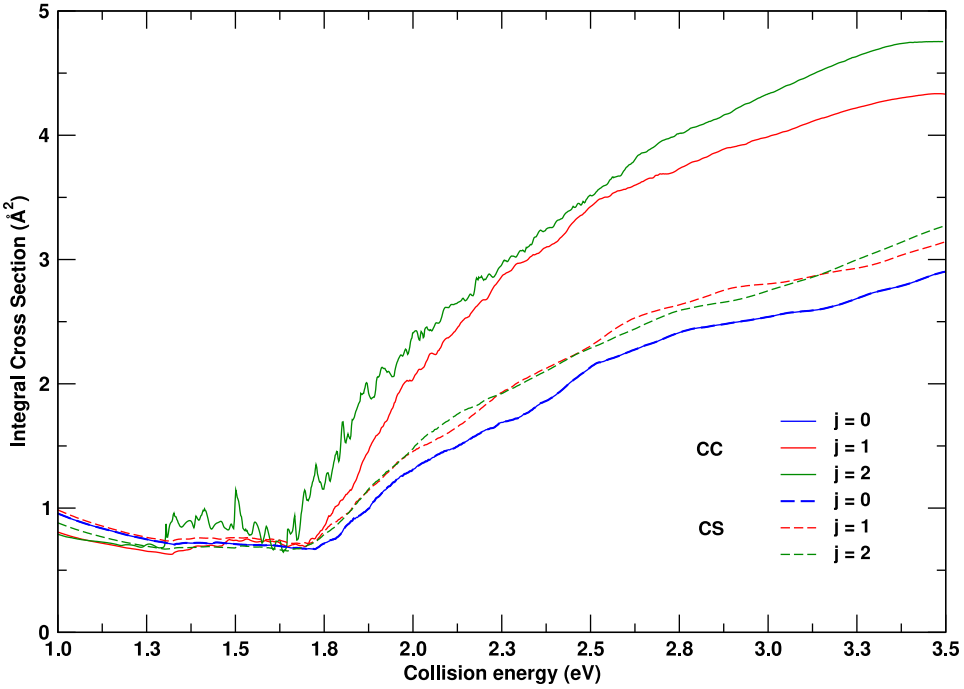

Fig. 7. Comparison of initial state-selected and energy-resolved integral cross sections, obtained from CC (solid line) and CS (dashed line) methods, for the K+$H_2(v = 2, j = 0–2)$ reaction as a function of collision energy.

product. For further understanding, the $(2J + 1)$ weighted probabilities for the K+$H_2(v = 2, j = 2)$ reaction as a function of J (see Fig S1), and $J\Omega$-dependent reaction probabilities for $j = 1$ (see Fig S2) are kept in the supporting information.

3.3. Integral cross sections and thermal rate constants

Here, we discuss the initial state-selected and energy resolved integral cross sections (ICSs) for the K + H_2 reaction in the ground electronic PES. The results are obtained by summing up all partial waves of J and its projection quantum number Ω with appropriate degeneracy weight factor, using Eq. (12) as described in Section 2. Fig. 7 represents the integral cross sections as the function of collision energy for different $j = 0–2$ levels of H_2 reagent obtained using the CC (solid line in the figure) and CS (dotted line in the figure) methods. The integral cross section results reveal a monotonically increasing pattern with increasing collision energy, and they attest that the reaction is of endothermic type. The oscillation observed in the reaction probabilities are still survived although mild in the cross section results at low collision energy, and the same is completely averaged out at higher energies. The reaction cross section from CC method is generally two-fold higher than that of CS results particularly at high collision energies (above 2.5 eV). The mild oscillations, as stated above, are surprisingly preserved better for $j = 2$ than for $j = 0$ and 1 by the CC approach. The ICS results clearly reveal the demand of higher energy for the reaction to occur, and thereby draw a conclusion that the reaction may be involved in a trivial tunneling of the heavy atom(K) via insertion path.

In order to validate the present result obtained from our TDWP calculation, we have compared the ICS for K + H_2(v = 0, 2, j = 0) system with other quantum mechanical results uses other PESs Li *et al.* [21] and Yuan *et al.* [22], shown in Fig. 8 for the collision energy range up to 1.6 to 2.0 eV. The collision energy threshold is clearly seen and numerous oscillation are seen in our result (CC method) and the ICS values reported by Li *et al.* are significantly high at low collision energies compared to Yuan *et al.* and the present study.

Now the important dynamical quantity, rate constant, is presented for the $K(^2S)$ + $H_2(X^1\Sigma_g^+)$ reaction in its ground electronic PES $(1^2A')$ and for the different reagent rotations (j), as shown in Fig. 9(a). The thermal rate constant $(k_{vj}(T))$ is calculated with the initial state-selected and by averaging the integral cross sections over the Boltzmann distribution of energy. As detailed above, a minimum second vibrational level $(v = 2)$ is required for H_2 reagent to meet the incoming K atom in its ground state. The rate constants obtained from the CC approach (solid line) are compared with the CS approximation method, represented in the figure as solid and dashed line, respectively. The CS rate constant values found to be high at very low temperatures ($\sim 1.4 \times 10^{-7}$ cm^3 s^{-1} molecule^{-1} for (2, 2) level) and then decreasing upon increasing temperature in the range of 10–5000 K. On the other hand, the CS method overestimates the rate results compared to that of the CC at low-T range, and then there is no noticeable change in the CC and CS rate coefficients at above 1000 K temperature.

Finally, averaging the initial state-selected rate quantities further by the thermal population of reagent rotational levels of the K + $H_2(v = 2, j = 0–2)$ reaction yield the state-averaged thermal rate constants, $k_{v=2}(T)$, presented in Fig. 9(b). In the figure, the Boltzmann state-averaged rate quantities for the temperature range of 10-1000K is well fitted to the Kooij form of the Arrhenius equation, i.e., $k(T) = \alpha \left(\frac{T}{300\text{K}}\right)^{\beta} \exp(-\gamma/T)$, and the fit is shown by dotted line. The fitting parameters for the CC(CS) rates are 8.72828×10^{-8}(8.6845×10^{-8}) cm^3 s^{-1} molecule^{-1}, 0.009(0.029), and 81.87(80.23) K, respectively. In conclusion, the CS findings (solid-red line) overestimates the CC result for the formation of KH products preceded by the H_2 depletion reaction. So, we believe that the present study may contribute to the astrophysical research and support to perform the state-specific dynamics of $K(^2S)$ + H_2 reaction from its ground electronic state which is experimentally challenging.

3.4. Kinematic effects on the KH_2 reaction dynamics

In this section, we made an effort to comprehend how the dynamics of the title reaction in the ground electronic state $(1^2A')$ are affected by the kinetic isotopic substituent. For the purpose, H atom is replaced

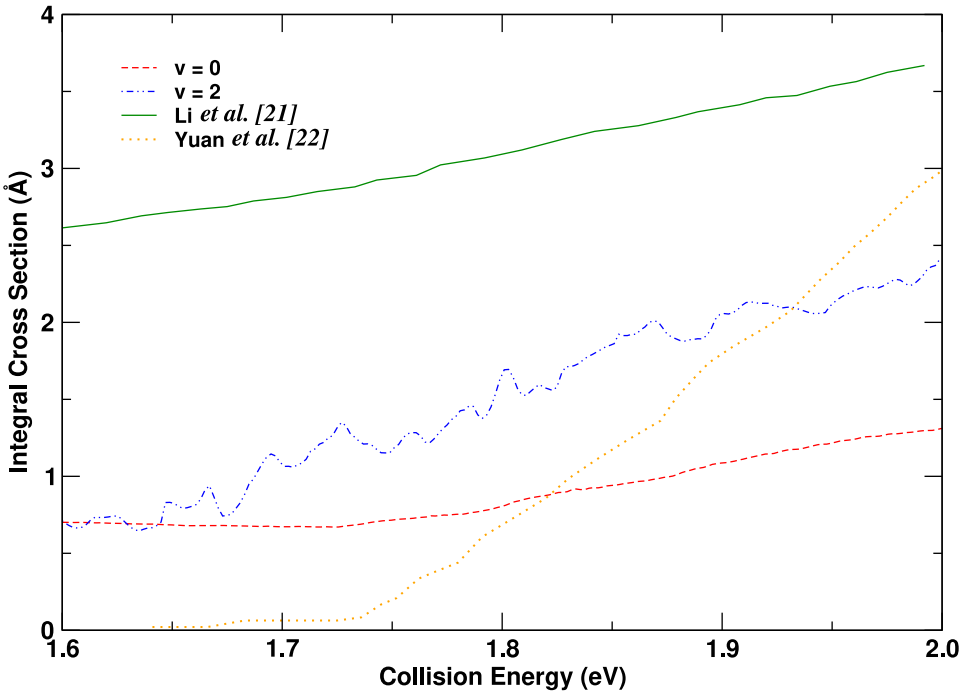

Fig. 8. Comparison of the energy-resolved integral cross section obtained from CC method with the reported cross sections employing other PESs Li *et al.* [21] ($v = 1$) and Yuan *et al.* [22] ($v = 2$).

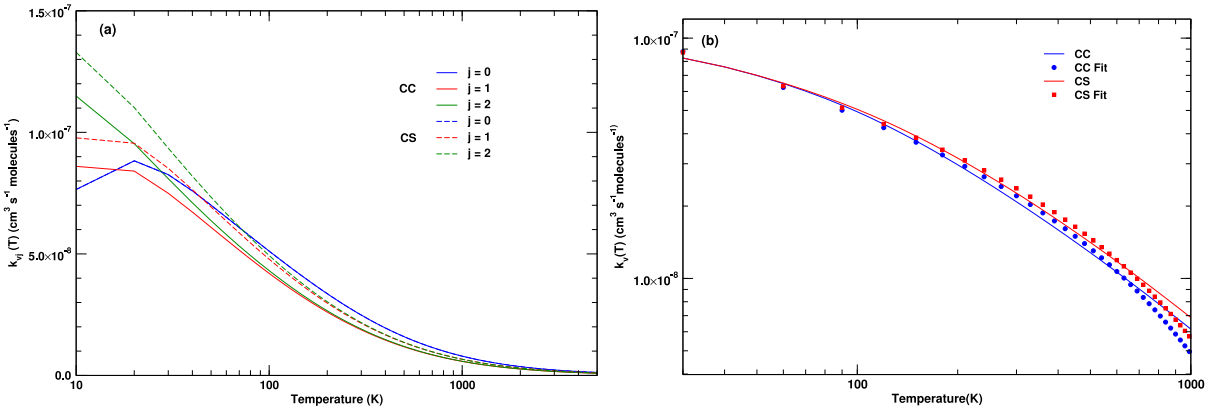

Fig. 9. (a) Initial state-selected thermal rate constants of the K + $H_2(v = 2, j = 0 - 2)$ reaction over the temperature range of 10–5000 K, obtained from the CC (solid line) and CS (dashed line) calculations. (b) The Arrhenius-like fit to the Boltzmann state-averaged rate constants for 10–1000 K. All axes are in logarithmic scale.

by its isotope deuterium (D) atom in the reactant channel resulting the three analogous collision systems as,

$$\begin{aligned} &K + DD \longrightarrow D + KD \qquad (S_1),\\ &K + HD \longrightarrow H + KD \qquad (S_2),\\ &K + HD \longrightarrow D + KH \qquad (S_3), \end{aligned}$$

and the parent collision (title) system is denoted as S_0. The reaction S_1 represents the KD formation via D_2 depletion, and $S_2(S_3)$ represents the KD(KH) formation via HD depletion.

The initial state-selected reaction probabilities and integral cross sections are calculated for the isotopic variants (S_i, $i = 1, 2, 3$) of the title system (S_0) using the Coriolis coupling technique, as outlined in Section 2. The Fig. 10 displays the reaction probabilities of S_i systems for the second vibrational level and excluding the rotational excitation, i.e., $v = 2, j = 0, J = 0$. The probability profile seen for the parent system (S_0) is completely distorted by the isotopic counterparts (S_i). It is noted that the KH product formation via HD depletion is closely achieved by the S_3 system on par with the parent system, but only at high collision energy ~3.2 eV for $v = 2$. In contrast, the KD formation via HD depletion in S_2 is observed with substantially low probability values than the parent system even at very high E_{col}. It is further noted that the D_2 depletion (S_1) shows better reactivity than the HD depletion (S_2) towards the formation of KD product. Additionally, the zero-point energy (ZPE) values of the reagent molecules (HD or D_2) play a significant role, i.e., heavier the isotopic substitution lowers the ZPE (see Table S1), and hence required more energy for bond dissociation which finally affects (lowers) the measured rate. Therefore, the isotopic substituents requires a few more (ro)vibrational levels of diatom in order to meet the K atom and reach the product (KH or KD) channel (see Fig. S3). Getting into more insights of the isotopic effects, we have calculated $|J\Omega\rangle$ dependent reaction probabilities of S_i systems using the CC approach, and presented the results in Fig. S4 (for $j = 1$) and S5 (for $j = 2$) of the supporting information.

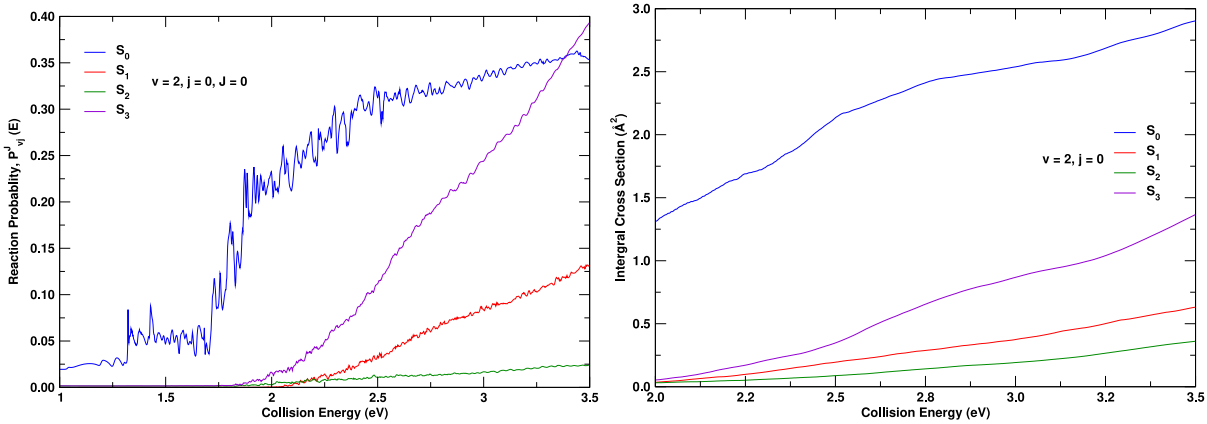

Fig. 10. Kinematics effects on reaction probabilities (left) and integral cross section (right) plotted as a function of collision energy for $v = 2, j = 0$ level of the reagent diatom.

The Fig. 10 (right panel) also displays the integral cross sections calculated for S_i systems compared with its parent system S_0 for the initial ($v = 2, j = 0$) level. It can be seen from figure that the reaction probability observations are carried over here by averaging out some oscillatory features. The cross section values are significantly higher for the formation of KH product than that of the KD product in that specified (v, j) level. It suggests the overall reactivity as, S_0(KH) > S_3(KH) > S_1(KD) > S_2(KD), and helps to draw a conclusion that the isotopic substitution significantly lowers the reactivity of the title reaction.

4. Summary

Here, we summarize the findings on the K(^2S) + $H_2(X\,^1\Sigma_g^+)$ reaction dynamics performed on the YDWLH-PES (ground electronic surface, $^2A'$) using the TDWP approach. The (ro)vibrational excitations of reagent H_2 is significantly influence the dynamics. The orientational effects also considered by means of including the Coriolis coupling terms (J and Ω quantum numbers) and reported the initial state-selected reaction probabilities, integral cross sections and rate constants. All partial waves of J up to 90 were required to obtain the convergence in cross section results up to the collision energy of 3.5 eV. In parallel, the dynamical results were also calculated within the CS approximation method and validated them. It reveals that the CS approximation overestimates the rate coefficients for the title reaction compared to the CC method.

Since the underlying PES is endoergic (~2.95 eV) with uphill profile, the H_2 reagent required at least a second vibrational level to reach the KH product channel, and hence the dynamics is significant only from $v = 2$ level. In a nutshell, the K + H_2 system requires a sufficiently high (ro)vibrational contribution of the reagent in combination with collisional energy, and also includes more orientations (high J and Ω) towards the selective formation of KH product. Further, the study of kinetic isotopic effects on the title system reports that the KH product formation is predominant than the KD formation via HD depletion reaction, and signifies the K + HD collision proceeds much faster than the other isotopologues.

CRediT authorship contribution statement

Santhakumar Yeswanth Kumar: Investigation, Methodology model, Visualization, Writing – original draft. **Natarajan Arumugam:** Formal analysis, Writing, Funding acquisition. **Abdulrahman I. Almansour:** Formal analysis, Writing, Resources. **Muhammed Jeneesh Kariyottu Kuniyil:** Formal analysis, Writing, Resources. **Ramanathan Padmanaban:** Conceptualization, Writing – review & editing, Supervision.

Declaration of competing interest

The authors declare that they have no known competing financial interests or personal relationships that could have appeared to influence the work reported in this paper.

Data availability

Data will be made available on request.

Acknowledgments

The first author (SYK) thanks Pondicherry University for the research fellowship. The computational facilities provided by the UGC-SAP under the Department of Special Assistance (DSA- I), New Delhi, are gratefully acknowledged. The project was supported by Researchers Supporting Project number (RSP2024R143), King Saud University, Riyadh, Saudi Arabia.

References

[1] T. Dunham Jr., Interstellar neutral potassium and neutral calcium, Publ. Astron. Soc. Pac. 49 (1937) 26–28.
[2] P. Stancil, S. Lepp, A. Dalgarno, The lithium chemistry of the early Universe, Astrophys. J. 458 (1996) 401–406.
[3] R. Padmanaban, S. Mahapatra, Time-dependent wave packet dynamics of the H+ HLi reactive scattering, J. Chem. Phys. 117 (14) (2002) 6469–6477.
[4] T. Roy, S. Mahapatra, Quantum dynamics of H+ LiH reaction and its isotopic variants, J. Chem. Phys. 136 (17) (2012) 174313.
[5] S. Bililign, P. Kleiber, Nascent rotational quantum state distribution of NaH (NaD) from the reaction of Na*(4 ^2P) with H_2, D_2, and HD, J. Chem. Phys. 96 (1)(1992) 213–217.
[6] S. Bililign, P. Kleiber, W. Kearney, K. Sando, Reactive collision dynamics of Na*(4 ^2P)+ H^2 and HD: Experiment and theory, J. Chem. Phys. 96 (1) (1992) 218–229.
[7] X. Huang, J. Zhao, G. Xing, X. Wang, R. Bersohn, The reaction of Cs (8 ^2P) and Cs (9^2P) with hydrogen molecules, J. Chem. Phys. 104 (4) (1996) 1338–1343. K.-C.
[8] Lin, R. Vetter, Alkali-hydrogen reactions, Int. Rev. Phys. Chem. 21 (3)(2002) 357–383.
[9] K.C. Lin, A.M. Schilowitz, J.R. Wiesenfeld, Collisional deactivation of potassium (5^2P_J) by molecular hydrogen. Identification of the primary quenching channel, J. Phys. Chem. 88 (26) (1984) 6670–6675.
[10] K.-C. Lin, H.-C. Chang, State-selective reaction of excited potassium atom with hydrogen molecule. K*+ H_2 → KH+ H, J. Chem. Phys. 90 (11) (1989) 6151–6156.
[11] H.-C. Chang, Y.-L. Luo, K.-C. Lin, Collisional deactivation of K (7s ^{2}S) and K (5d ^{2}D) by H_2, J. Chem. Phys. 94 (5) (1991) 3529–3536.
[12] Y.-L. Luo, K.-C. Lin, D.-K. Liu, H.-J. Liu, W.-T. Luh, Collisional deactivation for K in high-lying ^{2}S and ^{2}D states by H_2, Phys. Rev. A 46 (7) (1992) 3834.

[13] D.-K. Liu, K.-C. Lin, Rotational population distribution of KH (v=0, 1, 2, and 3) in the reaction of K ($5\,^2P_J$, $6\,^2P_J$, and $7\,^2P_J$) with H_2: Reaction mechanism and product energy disposal, J. Chem. Phys. 105 (20) (1996) 9121–9129.
[14] D.-K. Liu, K.-C. Lin, State-specific reaction and product energy disposal of electronically excited potassium with hydrogen molecule, J. Chem. Phys. 107 (11) (1997) 4244–4252.
[15] Y.-C. Hsiao, D.-K. Liu, H.-S. Fung, K.-C. Lin, Temperature effect on the deactivation of electronically excited potassium by hydrogen molecule, J. Chem. Phys. 113 (11) (2000) 4613–4619.
[16] L.-H. Fan, J.-J. Chen, Y.-Y. Lin, W.-T. Luh, Reaction of Rb (5^2D, 7^2S) with H_2, J. Phys. Chem. A 103 (10) (1999) 1300–1305.
[17] M.-L. Chen, W.-C. Lin, W.-T. Luh, Electronic to vibrational energy transfer between Rb ($5\,^2P_J$) and H_2, J. Chem. Phys. 106 (14) (1997) 5972–5978.
[18] J.-M. L'Hermite, G. Rahmat, R. Vetter, The Cs (7P)+ $H_2 \rightarrow$ CsH+ H reaction. I. Angular scattering measurements by Doppler analysis, J. Chem. Phys. 93 (1) (1990) 434–444.
[19] V. Cavero, J.-M. L'hermite, G. Rahmat, R. Vetter, Cs ($6D_{3/2}$)+ $H_2 \rightarrow$ CsH+ H reaction. IV. Rotationally resolved total cross sections, J. Chem. Phys. 110 (7) (1999) 3428–3436.
[20] T.-H. Wong, P. Kleiber, K.-H. Yang, Chemical dynamics of the reaction K*($5p\,^2$P)+ $H_2 \rightarrow$ KH (v=0; J)+ H: Electronic orbital alignment effects, J. Chem. Phys. 110 (14) (1999) 6743–6748.
[21] W. Li, X. Wang, H. Zhao, D. He, Non-adiabatic dynamics studies of the K ($4p\,^2$P)+ H_2 ($X^1\Sigma$) reaction based on new diabatic potential energy surfaces, Phys. Chem. Chem. Phys. 22 (28) (2020) 16203–16214.
[22] J. Yuan, Z. Duan, S. Wang, J. Liu, K. Han, Significant effects of vibrational excitation of reactant in K+ $H_2 \rightarrow$ H+ KH reaction based on a new neural network potential energy surface, Phys. Chem. Chem. Phys. 20 (31) (2018) 20641–20649.
[23] R. Kosloff, Time-dependent quantum-mechanical methods for molecular dynamics, J. Phys. Chem. 92 (8) (1988) 2087–2100.
[24] R. Kosloff, Propagation methods for quantum molecular dynamics, Annu. Rev. Phys. Chem. 45 (1) (1994) 145–178.
[25] D. Zhang, J. Zhang, Time-dependent quantum dynamics for gas-phase and gas-surface reactions, in: R. Wyatt, J. Zhang (Eds.), Dynamics of Molecules and Chemical Reactions, Marcel Dekker, 1996, p. 231.
[26] J.Z.H. Zhang, Theory and Application of Quantum Molecular Dynamics, World Scientific, 1999.
[27] N. Balakrishnan, C. Kalyanaraman, N. Sathyamurthy, Time-dependent quantum mechanical approach to reactive scattering and related processes, Phys. Rep. 280 (2) (1997) 79–144.
[28] A.J. Meijer, E.M. Goldfield, Time-dependent quantum mechanical calculations on H+O_2 for total angular momentum J> 0, J. Chem. Phys. 108 (13) (1998) 5404–5413.
[29] E.M. Goldfield, A.J. Meijer, Time-dependent quantum mechanical calculations on H+ O_2 for total angular momentum J> 0. III. Total cross sections, J. Chem. Phys. 113 (24) (2000) 11055–11062.
[30] T.E. Carroll, E.M. Goldfield, Coriolis-coupled quantum dynamics for O (1D)+ $H_2 \rightarrow$ OH+ H, J. Phys. Chem. A 105 (11) (2001) 2251–2256.
[31] T. González-Lezana, O. Roncero, P. Honvault, J.-M. Launay, N. Bulut, F. Javier Aoiz, L. Bañares, A detailed quantum mechanical and quasiclassical trajectory study on the dynamics of the H^++ $H_2 \rightarrow H_2$+ H^+ exchange reaction, J. Chem. Phys. 125 (9) (2006) 094314.
[32] R.T. Pack, Space-fixed vs body-fixed axes in atom-diatomic molecule scattering. sudden approximations, J. Chem. Phys. 60 (2) (1974) 633–639.
[33] P. McGuire, D.J. Kouri, Quantum mechanical close coupling approach to molec-ular collisions. j_z-conserving coupled states approximation, J. Chem. Phys. 60 (6) (1974) 2488–2499.
[34] S.Y. Kumar, P. Sundaram, R. Padmanaban, Coriolis coupling and isotopic effects on the quantum dynamics of H(^{2}S) NaH($X^1\Sigma^+$) reaction, Eur. Phys. J. D. 75 (2021) 1–18.
[35] S. Mahapatra, N. Sathyamurthy, Negative imaginary potentials in time-dependent quantum molecular scattering, J. Chem. Soc., Faraday Trans. 93 (5) (1997) 773–779.
[36] J. Kerr, KP huber and g. Herzberg, molecular spectra and molecular structure: IV constants of diatomic molecules: Von Nostrand—Reinhold, New York, 1979, p. 716.
[37] R. Johnson, Computational Chemistry Comparison and Benchmark Database, NIST Standard Reference Database 101, National Institute of Standards and Technology, 2016.